

A numerical study of dynamic behavior of the molten pool in laser welding of aluminum alloy

Menghua Ma^{1,*}

¹ College of Information and Mechatronics Engineering, Zhengzhou Business University, Henan 451200, PR China

Received: 10 February 2025 / Accepted: 31 October 2025

Abstract. During the laser welding process of aluminum alloy, the high reflectivity of aluminum alloy to laser and the severe fluctuation of the keyhole lead to highly unstable energy absorption, which readily induces defects such as spatter and porosity. Furthermore, the multi-physical field coupled dynamic behaviors within the molten pool, involving heat transfer, fluid flow, phase transformation, and element evaporation, are difficult to capture and quantify, resulting in a lack of precise theoretical guidance for this process. To address these issues, a multiple-reflection laser absorption model for the keyhole in the aluminum alloy laser welding molten pool was established. Basic assumptions were applied to the laser welding process to simplify the calculation of the molten pool mathematical model. The governing equations for the laser welding molten pool were established. Finally, the laser welding molten pool process was simulated. Experimental results demonstrate that employing a laser incident angle of 30° reduces the molten pool flow velocity by approximately 40%, effectively suppressing the spatter phenomenon. When the welding speed is increased to 8.0 m/min, the escape efficiency of molten pool bubbles is enhanced by 50%, and the uniformity of element diffusion is significantly improved. The comprehensive optimization of parameters can improve weld formation quality by more than 35%. The study provides an effective numerical analysis tool for understanding keyhole dynamics and molten pool behavior in aluminum alloy laser welding, significantly enhancing the comprehension of defect formation mechanisms. The established models and optimization results can offer a theoretical basis and parameter design guidance for the development of high-quality and high-efficiency aluminum alloy laser welding processes.

Keywords: Aluminum alloys / welding molten pool / dynamic behavior

1 Introduction

As a high-precision and high-efficiency welding technology [1,2], the dynamic behavior of the molten pool during the laser welding process is complex and variable, which directly affects the welding quality, weld morphology and the microstructure of the material. Among them, aluminum alloy, as a lightweight and high-strength metal material, has a wide range of applications in aerospace, automotive manufacturing and other fields. However, there are some challenges in the laser welding process of aluminum alloys, such as the formation of welding defects such as pores and cracks, as well as the instability of mechanical properties of welded joints. Therefore, research on laser welding of aluminum alloys has always been highly concerned. The study of dynamic behavior of molten pool is an important direction. A study analyzed the influence of different laser powers on the morphology and flow behavior

of the molten pool in aluminum alloy laser welding through numerical simulation. It was found that with the increase of laser power, the morphology of the molten pool changed from a droplet shape to an ellipse, and the surface of the weld changed from a convex shape to a flat or concave shape. The dynamic behavior of the molten pool has a direct impact on the formation of welding defects. Therefore, studying the dynamic behavior of the molten pool in aluminum alloy laser welding through numerical simulation technology has theoretical and engineering practical value [3]. By using computer simulation calculations, the dynamic process of the molten pool under different welding conditions can be simulated, revealing the physical and chemical phenomena inside the molten pool, such as heat conduction, fluid flow, and changes in the shape of the molten pool. This not only helps to analyze the behavior of the molten pool, but also provides insights into the underlying physical mechanisms. This not only helps to understand the intrinsic mechanism of the molten pool behavior, but also provides a theoretical basis for optimizing welding process parameters, predicting welding

* e-mail: 18236850640@163.com

defects and improving welding quality. In addition, numerical simulation also has the advantages of low cost, short cycle time, repeatability and so on, which can evaluate and compare multiple welding schemes in a short time, and provide powerful support for process optimization in actual production. Therefore, the numerical simulation of the dynamic behavior of the laser welded molten pool has important theoretical significance and practical application value.

Peng et al. [4] proposed a three-dimensional morphological features based on the impact of the study of the dynamic behavior of the laser welding molten pool program, first of all, three-dimensional morphological characterization of the laser welded filler, to obtain the significant features of the laser welding molten pool flow, combined with the principle of fluidics, with the With the increase of driving force, the original maintenance hole also increases, and the flow tendency of the hole wall surface of the laser welding becomes stronger. Huang et al. [5] aluminum alloy as the experimental material, the use of high-speed photography on the laser welding process shooting, according to the shooting results of the flow of the laser scanning welding and the traditional single-laser welding to analyze the acquisition of plasma fluctuation characteristics, the experimental results show that the situation of oscillating laser welding than the traditional single Laser light velocity stability, when the pressure is reduced, can effectively improve the overall stability of laser scanning welding. Yang et al. [6] using numerical software Fluent, 10 mm thick 2219 aluminum alloy electron beam welding for three-dimensional transient simulation. Analyze the change rule of eddy currents in the molten pool after the electron beam welding into a quasi-steady state and the reasons for this, and discuss the interaction between the electron beam and the keyhole wall surface. Wu et al. [7] takes 2 mm thick 7075-T6 aluminum alloy sheet as the object of study, establish a low-frequency cosine oscillation scanning laser welding heat transfer model. A comparative study was conducted on low-frequency oscillation scanning laser welding through numerical simulation. Based on the above research background, considering that there are other factors affecting the welding quality of alloys when applying laser welding technology, such as the laser incidence angle and welding speed, it is proposed to study the dynamic behavior with the help of numerical simulation technology [8,9] using aluminum alloys as experimental materials, and adopting different laser incidence angles and welding speeds. The simulation results show that the laser incidence angle affects the fluid flow rate in the molten pool of aluminum alloys when laser welding is used. When the laser incidence angle is positive, the spattering phenomenon is suppressed, and when the laser incidence angle is negative, the spattering phenomenon is promoted.

2 Test materials and methods

2.1 Test materials

– Analysis of the properties of the parent material

Table 1. Chemical composition of base material.

Chemical composition	Content/%
Cu	0.18
Zn	Less than 0.01
Si	0.64
Mn	0.21
Fe	0.25
Mg	0.37
Ti	0.03
Al	Bal

Table 2. Details of base material mechanics.

Mechanical details	Values
Yield strength/MPa	315
Tensile strength/MPa	586
Elongation at failure/%	25

Table 3. Chemical composition of welding wire.

Chemical composition	Content/%
Fe	0.41
Ti	0.16
Cr	0.17
Zn	More than 0.3
Mg	4.85
Mn	0.96
Cu	0.06
Si	0.26

In this paper, the welding of raw materials used for 6005A aluminum alloy material. The chemical composition of the substrate is shown in Table 1.

Details of the mechanical properties of this parent material are shown in Table 2.

– Analysis of welding wire properties

In order to make the welded joints to achieve more ideal results, when choosing the parent material, consider the 6005A aluminum alloy due to its properties being closer to those of the 6082 aluminum alloy electrode. The chemical composition of welding wire is shown in Table 3.

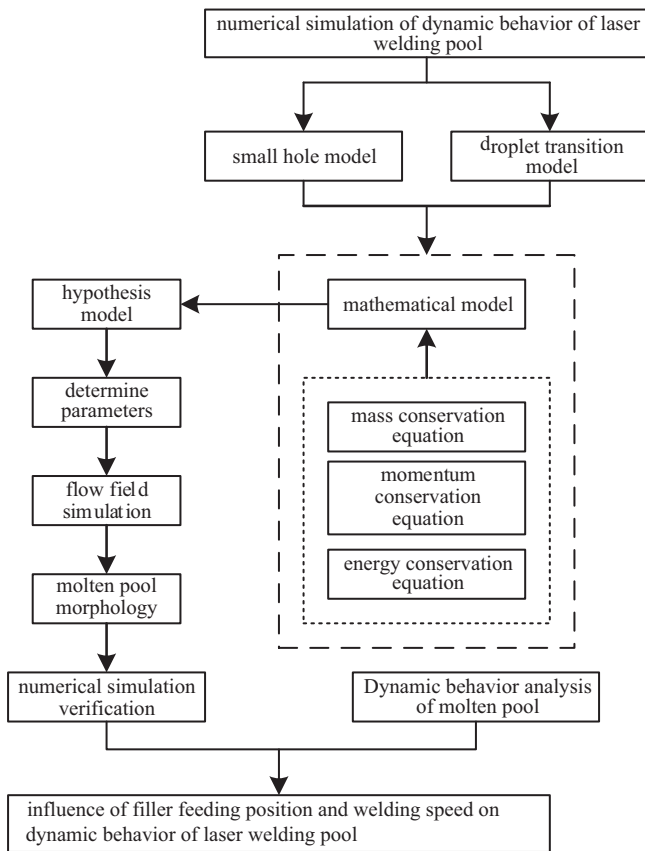
The wire has a tensile strength of 295 MPa.

2.2 Test equipment and methods

For the laser welding process [10,11], the equipment used included a BPSL-K300 model welder, a fiber laser and a robot with supporting fixtures. The specific laser welding parameters are shown in Table 4.

Table 4. Welding parameters.

Parameter name	Parameter size	Parameter name	Parameter size
Focus	125 mm	Optical filament spacing	1 mm
Welding gun inclination angle	30°	Defocus amount	-1 mm
Optical fiber core diameter	150 μm	Butt clearance	0.34 mm
Collimation	50 mm		

**Fig. 1.** Modeling process.

2.3 Laser welding melt pool modeling

A combination of laser welding [12] experiment and simulation was used to study the dynamic behavior of the laser welded molten pool, and the specific modeling flow is shown in Figure 1.

In the laser welding [13–15] process, high temperatures make the metal surface prone to oxidation when exposed to atmospheric oxygen. Inert gases such as argon, helium, etc., because of its chemical inactivity, can form a protective atmosphere in the welding area, preventing oxygen and metal contact, thus ensuring the purity of the weld metal. Welding of different inert gases, gas-saving combination shown in Table 5.

The diameter and length of the welding pin used in the welding process is 3 mm, the diameter of the shoulder is 11 mm, the tilt angle of the welding head used in welding is 2.5°, the rotational speed of the welding head is set at

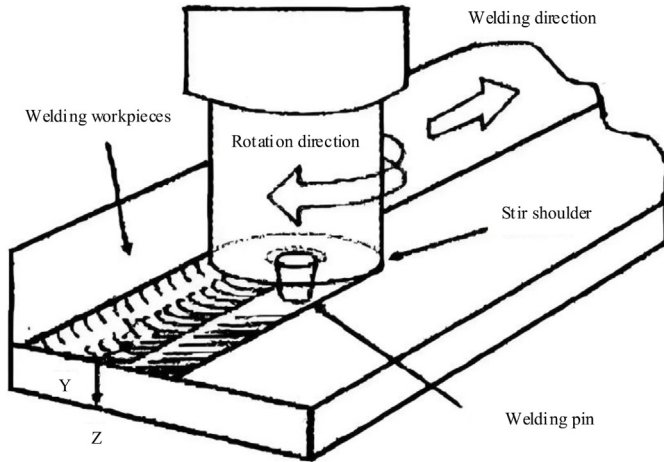
1250 r/min, the welding head needs to be pressed down during welding, the amount of downward pressure needs to be controlled in the range of 0.1 mm, the welding pin is inserted into the base material and the wire between the welding pin is preheated for 5 s [16]. The detailed welding procedure is as follows:

- Fix the 6005A aluminum alloy material to be welded on the working platform to ensure that the material will not move or be deformed during the welding process.
- Clean 6005A aluminum alloy material surface, remove oil, oxide film and other impurities to improve the welding quality.
- Start the laser welding equipment.
- Insert the laser welding head slowly into the joint of the 6005A aluminum alloy to be welded, and the shoulder of the welding head is closely connected to the surface of the aluminum alloy.
- When the welding head is in full contact with the 6005A aluminum alloy material and reaches a stable state, it starts to feed the movement in the welding direction at a constant welding speed.
- The welding head moves in the direction of the weld seam during the welding process, stirring and squeezing the material. This process helps to eliminate defects in the weld and improve the quality of the weld. As the weld head moves, the temperature gradually decreases and the softened material cools and solidifies to form the final weld.
- After the welding is completed, the welding head stops working and is slowly removed from the aluminum alloy material.

The welding tool used in this study combines the typical characteristics of friction stir welding. Traditional laser welding mainly forms a molten pool through the interaction between laser and material. However, this study adopts a composite welding mechanism of “laser preheating + mechanical stirring”, which generates frictional heat during rotation by tightly contacting the large-diameter shoulder with the workpiece surface, forming a stable heat affected zone. This can not only assist in the laser preheating effect, but also break down the surface oxide film of aluminum alloy through mechanical action, improving wettability. The use of small-diameter stirring needles can accurately control the heat input. After laser preheating softens the substrate, the material’s plastic flow is promoted through the shear action of the stirring needle, achieving uniform mixing of the microstructure. It is suitable for materials such as 6005A aluminum alloy that are easily oxidized and sensitive to heat.

Table 5. Different inert gas.

Gas selection	Argon	Argon:helium	Argon:helium:nitrogen	Argon:helium
Ratio	1	7:3	7:2.9:0.1	5:5
Welding speed/(cm/min)	5.00	7.00	7.50	9.90
Gas flow/(L/min)	15.00	15.00	15.00	15.00
No	Inert gas knots 1	Inert Gas Node 2	Inert gas node 3	Inert gas knots 4

**Fig. 2.** Welding process diagram.

The schematic diagram of the welding process is shown in Figure 2.

The composite motion of “rotation+movement” of welding tools is similar to the friction stir welding process, but its mechanism of action is fundamentally different. The friction stir welding process relies on frictional heat generation, and in this study, laser preheating provided the basic heat, while mechanical stirring mainly promotes material flow. This synergistic effect significantly improves energy utilization efficiency. By precisely controlling the downward pressure, a unique “vortex like” material flow pattern is formed under the action of the tilt angle of the stirring head, effectively eliminating defects such as pores and incomplete fusion.

2.4 Basic assumptions of the laser welding molten pool

The laser welding process [17,18] is a complex process in practice, involving a variety of physical reactions, and in order to reduce the complexity of laser welding simulations, the following assumptions were made:

- Neglecting the chemical reaction between the laser welded molten pool and the gases in the alloy pores;
- Neglecting the effect of plasma on laser welding;
- The alloy material is assumed to be isotropic;
- The relationship between the laser welded molten pool and the small holes is symmetrical with respect to the weld seam.

2.5 Laser welding heat transfer control

During laser welding [19,20], the chemical elements contained in the aluminum alloy will react physically under the action of the laser, and due to the different densities of the aluminum alloy in the gaseous and liquid phases, the velocity will be changed abruptly, and the controlling equations, which are the equations for the conservation of mass, momentum, and energy, respectively, have been established [21].

The mass conservation equation is:

$$\frac{\partial \rho'}{\partial t} + \nabla n(\rho V) = M \quad (1)$$

Among them, ρ' denotes the density of the metal. M denotes the quality source term, V represents the volume of the metal, t indicates the time. ∇ denotes the gradient operator.

Conservation of Momentum Equation:

$$\begin{aligned} \rho \left[\frac{\partial u}{\partial t} + (u - u_0) \frac{\partial u}{\partial x} + v \frac{\partial u}{\partial y} + w \frac{\partial u}{\partial z} \right] &= - \frac{\partial p}{\partial x} \\ + \mu \left(\frac{\partial^2 u}{\partial x^2} + \frac{\partial^2 u}{\partial y^2} + \frac{\partial^2 u}{\partial z^2} \right) + F_x \\ \left[\frac{\partial v}{\partial t} + (u - u_0) \frac{\partial v}{\partial x} + v \frac{\partial v}{\partial y} + w \frac{\partial v}{\partial z} \right] & \\ = - \frac{\partial p}{\partial y} + \mu \left(\frac{\partial^2 v}{\partial x^2} + \frac{\partial^2 v}{\partial y^2} + \frac{\partial^2 v}{\partial z^2} \right) + F_y \\ \rho \left[\frac{\partial w}{\partial t} + (u - u_0) \frac{\partial w}{\partial x} + v \frac{\partial w}{\partial y} + w \frac{\partial w}{\partial z} \right] & \\ = - \frac{\partial p}{\partial z} + \mu \left(\frac{\partial^2 w}{\partial x^2} + \frac{\partial^2 w}{\partial y^2} + \frac{\partial^2 w}{\partial z^2} \right) + F_z \end{aligned} \quad (2)$$

Where, ρ represents the density of the welding unit, μ represents the dynamic viscosity coefficient of the metal, μ_0 represents the welding speed, u , v and w represent the three directional components of the fluid speed, p represents the pressure in the fluid, and F_x , F_y and F_z represent the momentum source term.

Energy Conservation Equation:

$$\begin{aligned} \rho \left[\frac{\partial H}{\partial t} + (u - u_0 + v + w) \frac{\partial H}{\partial (x + y + z)} \right] \\ = \frac{\partial}{\partial (x + y + z)} \left(k \frac{\partial T}{\partial (x + y + z)} \right) + F_v \end{aligned} \quad (3)$$

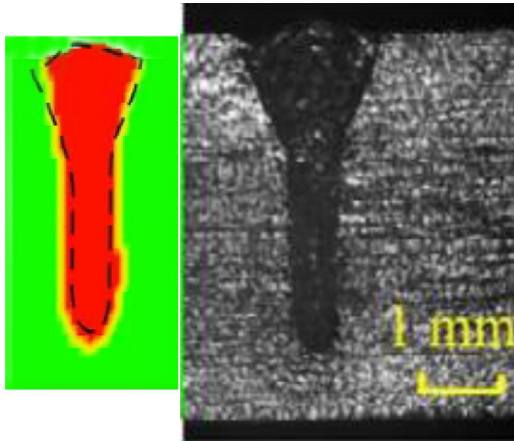


Fig. 3. Comparison between simulation model and actual test results.

Where, k denotes the thermal conductivity of the fluid, H denotes the enthalpy of mixing, T denotes time, F_v denotes the internal heat source term.

2.6 Laser welding simulation test and validation

The customized function was used to simulate the laser welding in real time by combining with the hydrodynamic software. In the dynamics software MEDYNA, the design of the initial parameters: laser power of 3600 W, laser defocus amount of 1 mm, protective gas flow rate of 20 L/min; boundary conditions: simulation model of the upper and lower surfaces for the free-flow boundary conditions, the side of the continuous boundary conditions; kinetic energy loading source: The fortran is used to write the program of laser heat source, heat conduction and heat convection between the surface and metal vapor, and the recoil pressure related model acting on the surface of the keyhole. After initialization, the calculation begins.

The numerical simulation uses ANSYS Fluent 2021 R1 as the main solving platform, coupled with self-developed Fortran UDFs to achieve multi physics field coupling. The computational domain adopts an unstructured tetrahedral mesh, locally densified to $20\ \mu\text{m}$ in the melt pool area, with 5 layers of prismatic mesh set in the boundary layer, the first layer is $5\ \mu\text{m}$ high, and the total mesh size is about 2.8 million. When the grid size increases from 2.4 million to 3.2 million, the change in melt pool size is less than 2%. The solver adopts the Pressure Based algorithm with a time step of 1×10^{-5} s to ensure that the Courant number is less than 1. The convergence criteria are set as follows: energy equation residual $< 1 \times 10^{-6}$, momentum equation residual $< 1 \times 10^{-5}$, continuity equation residual $< 1 \times 10^{-4}$, and the physical quantity fluctuation at each monitoring point is required to be less than 1%.

An aluminum alloy weld sample was selected, the weld cross-section was ground and polished, put into the etching solution (concentrated hydrochloric acid: concentrated nitric acid = 3: 1) for 20 s, then rinsed and blown dry, observed under the microscope, and the weld cross-section image was obtained, and compared with the results of the simulation model, and the results are shown in Figure 3.

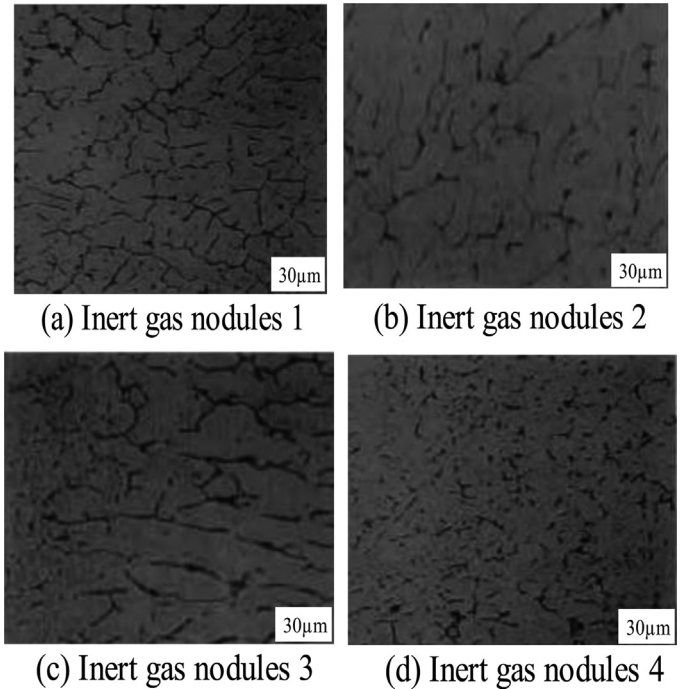


Fig. 4. Microstructure evolution under different inert gas atmospheres.

3 Test results and analysis

3.1 Micro-morphology of welded joint organization evolution under different inert gas throttles

The microstructure changes of laser welded joints are shown in Figure 4.

The base metal and wire unchanged, using the same welding method, only the shielding gas is different, the inert gas gas 4 welding weld micro-morphology in the organization of the smallest grain. Therefore, the choice of inert gas gas 4 to realize the welding.

3.2 Effect of different laser incidence angles on the dynamic behavior of the molten pool

In laser welding, in order to protect the laser equipment, to avoid interference between the laser head and the weldment, the laser head will be adjusted to a certain degree of deflection, which produces a different angle of laser incidence, the laser incidence angle will affect the morphology of the laser welded molten pool, which further affects the quality of the weld. The fluid flow image of the molten pool was obtained by eddy current thermography. The model MOI eddy current thermal imaging device is selected, which can adapt to the complex detection environment, with a field of view range of $25\ \text{mm}/\text{m}^2$, a data transmission speed of 100 nm/s, and the ability of pattern and paint penetration; its excitation current is up to 400 A, the excitation frequency interval is [150, 400] kHz, and the excitation time is 180 ms ; Video data can be stored in SD card, with flexible steering probe head, can realize the detection of different positions of the imaging.

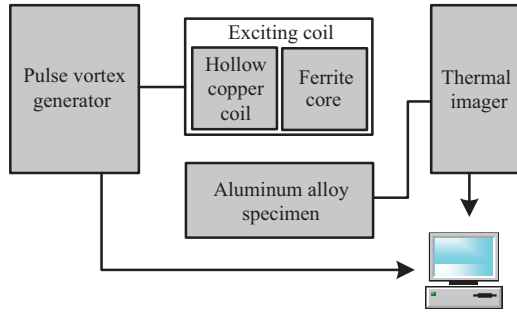


Fig. 5. Structural diagram of eddy current thermal imaging device.

The eddy current thermal imaging device mainly combines two technologies, infrared thermal imaging and eddy current detection, eddy current thermal imaging technology can detect shallow air holes as small as 1 mm depth and does not need to be in contact with the detected material, and can quickly collect thermal image sequences and adapt to the complex detection environment, which is suitable for inspection at the construction site. The structure of the eddy current thermal imaging device is shown in [Figure 5](#).

As shown in [Figure 5](#), the eddy current thermal imaging device mainly consists of a pulsed eddy current generator, an excitation coil, a thermal imager, etc. Among them, the excitation coil consists of a hollow copper coil and a ferrite core. Among them, the excitation coil includes hollow copper coil and ferrite core. The eddy current thermal imaging device is activated by the electrical signal generated by the pulsed eddy current generator, at this time, high-frequency alternating current is introduced into the hollow copper coil, generating an alternating magnetic field; the ferrite core generates a magnetic field aggregation, and at the same time, the magnetic field aggregation is transmitted to the target specimen through the magnetic circuit between the two magnetic poles.

The laser incidence angles were set to 30° and -30° , and the fluid flow images of the molten pool were obtained by eddy current thermography as shown in [Figure 6](#).

When the laser incident angle is 30° , the counterclockwise vortex occurs above the melt pool, and the clockwise vortex exists below the melt pool, and the fluid flow inside the melt pool is relatively smooth. When the laser incident angle is -30° , there are mainly clockwise vortices in the melt pool, the fluid flow inside the melt pool is more intense, and the convection effect at the top and bottom of the melt pool is not enough.

From the longitudinal cross-section of the laser welding pool, it can be seen that the flow field of the laser welding pool at different laser incidence angles has a very significant difference. Combined with the recoil pressure to analyze, laser incidence angle of 30° , the flow inside the melt pool is weak, the back wall of the keyhole of the high-temperature liquid metal diffusion is slower, slower heat dispersion; on the contrary, the angle of incidence of -30° , the melt pool inside the flow of fast, fast heat dispersion, vertical downward force on the back wall of the keyhole of the

high-temperature liquid metal to exert a downward pressure, the vertical upward force exerts an upward pressure in the combination of the force of the spatter phenomenon. Under the action of the combined force, the splash phenomenon occurs. Therefore, when the laser incident angle is positive, the spattering phenomenon can be reduced to a certain extent, while when the laser incident angle is negative, the spattering phenomenon is more likely to occur.

3.3 Effect of laser welding speed on the dynamic behavior of the laser welded molten pool

3.3.1 Influence of laser welding speed on the escape of gas bubbles from the molten pool

Whether the bubble can escape from the molten pool directly depends on the flow field speed and welding speed in the laser welding molten pool. Combined with the results of laser welding experiments on aluminum alloys, we obtained the flow field in the cross-section of the molten pool, conducted two sets of experiments.

During low-speed welding at 4.0 m/min, the greater the impact on the keyhole, the stronger the fluctuations, resulting in a large number of bubbles and corresponding changes in the flow trend in the melt pool. At a high welding speed of 8.0 m/min, the stability of the keyhole is significantly improved, the bubbles in the molten pool are significantly reduced, and the bubbles move to the top of the molten pool with the flow in the molten pool field. The dynamic behavior of bubble escape in the molten pool at different welding speeds is shown in [Figure 7](#).

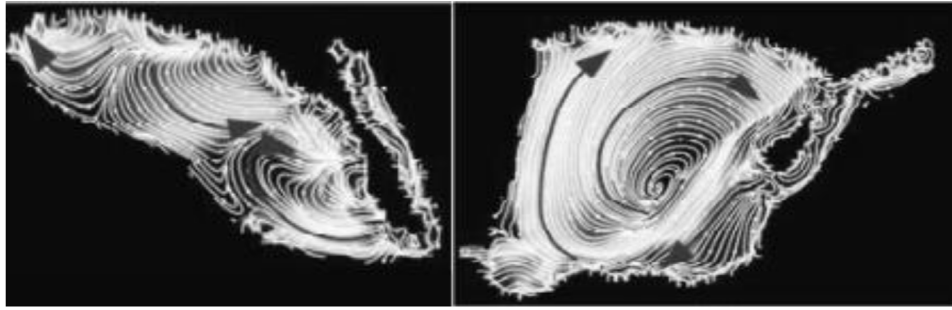
According to the results in [Figure 7](#), the laser welding speed was adjusted to specify the bubble escape process. The flow field in the longitudinal section of the molten pool at different welding speeds is shown in [Figure 8](#).

It can be seen that the eddy current flow area at the bottom of the molten pool decreases obviously at low welding speed. When the welding speed is high, reaching 8.0 m/min, the fluid flow area increases and the bubbles are easier to escape.

3.3.2 Effect of laser welding speed on elemental diffusion uniformity in the molten pool

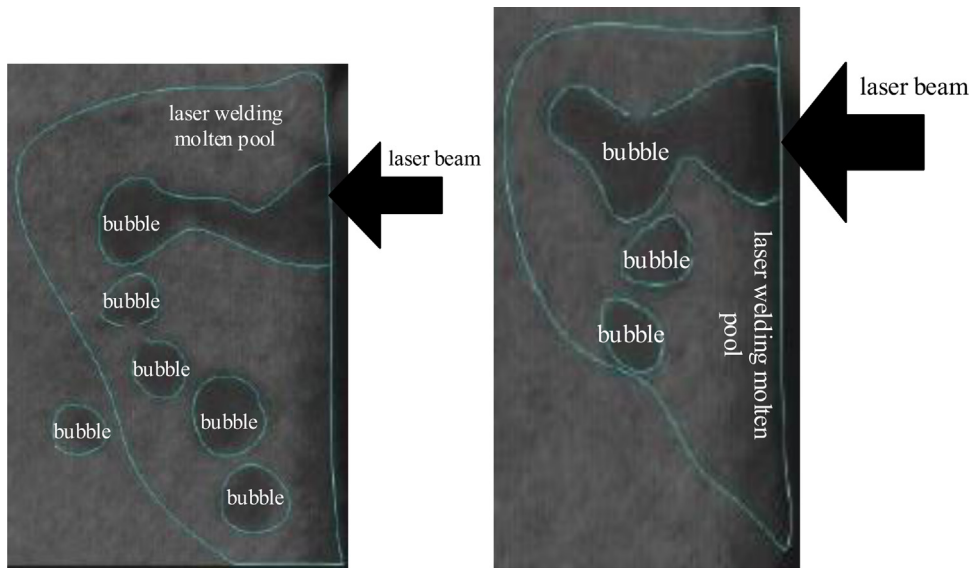
In the process of laser welding, the flow trajectory in the dynamic flow field of the molten pool plays a crucial role in the uniformity of element diffusion in the molten pool. This is because the uniformity of element diffusion directly affects the quality of welding, and the flow trajectory, as a key characteristic of the dynamic flow field in the melt pool, is largely determined by factors such as shape, direction, and velocity, which determine the diffusion mode and final uniformity of elements in the melt pool.

In view of this, in order to further study and accurately analyze the information of the molten pool flow field, researchers have adopted an effective method, which is to intercept the distance of the front wall of the small hole as the research entry point. By studying this specific location, many key data and characteristics about the flow field



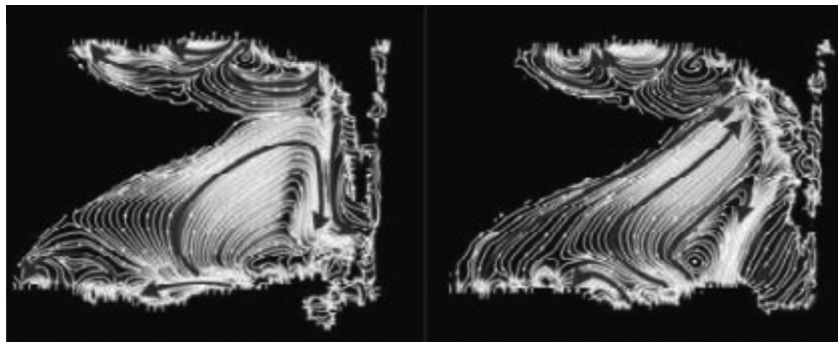
(a) The incident angle of laser is 30° (b) The incident angle of laser is -30°

Fig. 6. Flow field distribution of dynamic behavior of laser welding pool.



(a) When the welding speed is 4m/min(b) When the welding speed is 8m/min

Fig. 7. Dynamic behavior in laser welding pool.



(a) When the welding speed is 4m/min(b) When the welding speed is 8m/min

Fig. 8. Longitudinal section flow field of laser welding pool.

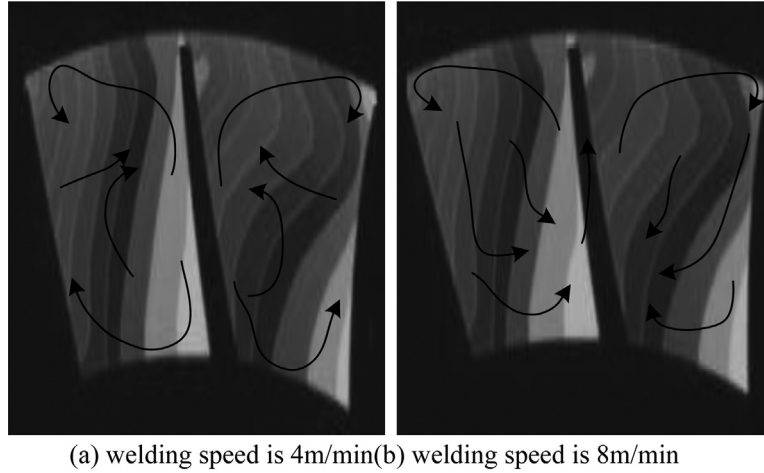


Fig. 9. Cross-sectional flow field.

Table 6. Analysis results of element diffusion energy spectrum points in weld zone under different welding speeds (atomic fraction,%).

Welding speed m/min	Test points	Si	Fe	Mg
4	1	54.21	14.82	9.03
	2	52.26	16.11	9.99
	3	53.68	15.96	8.61
8	1	55.2	16.33	8.51
	2	55.41	16.38	8.54
	3	55.91	15.94	8.61

of the melt pool can be obtained, providing strong support for a comprehensive understanding of the physical processes inside the melt pool.

Figure 9 visually illustrates the flow field in the cross-section of the molten pool under different welding speed conditions. Specifically, the flow field states presented here are at welding speeds of 4.0 m/min and 8.0 m/min. Different welding speeds can cause a series of complex physical changes inside the molten pool. Through careful observation and analysis of Figure 9, we can clearly see the differences in the morphology, flow direction, and velocity distribution of the molten pool flow field under these two different welding speeds. This provides a visual basis for further exploring the intrinsic relationship, as well as their impact on the uniformity of element diffusion in the molten pool.

Three points in the weld were randomly selected and analyzed for the diffusion energy spectra of each element, and the results are shown in Table 6 below.

Based on the above results, a significant difference can be clearly identified. Under different welding speeds, the dynamic fluid characteristics of the molten pool exhibit significantly different behaviors. When the welding speed is set to 4.0 m/min, the dynamic fluid characteristics of the molten pool are in a relatively

stable state. At this point, the fluid flow inside the melt pool is relatively gentle, and the overall flow trend is not very prominent.

However, when the welding speed was increased to 8.0 m/min, there was a significant change in the situation. Compared to a welding speed of 4.0 m/min, the dynamic fluid characteristics of the molten pool become stronger at a welding speed of 8.0 m/min. The fluid inside the melt pool exhibits a more active flow pattern, and the overall flow trend is also more significant. This change indicates that the increase in welding speed has a positive impact on the dynamic fluid characteristics of the melt pool, making the material exchange and energy transfer inside the melt pool more active, which may have a series of different effects on the welding quality and welding effect.

Comparing the elemental diffusion energy spectra in the weld zone, it can be found that the difference in the content of Si is 1.95% and the difference in the content of other elements is 1.29% and 1.38% at a welding speed of 4.0 m/min, while the difference in the content of Si is 0.71% and the difference in the content of other elements is even smaller at 8.0 m/min, which is less than 1%. This also indicates that this flow trend is favorable to the diffusion of elements, which further improves the uniformity of element diffusion inside the molten pool.

To summarize, the laser incidence angle affects the fluid flow in the molten pool. A positive laser incidence angle reduces the fluidity and suppresses the spattering phenomenon, while a negative laser incidence angle enhances the fluidity and makes it easy to produce spattering. When the welding speed is increased, the stability of the keyhole is improved, the flow area is larger, and the bubbles are reduced. When the welding speed is larger, it also has a promotion effect on the uniformity of element diffusion. Therefore, it is beneficial to improve the quality of weld formation by appropriately increasing the laser incidence angle and welding speed.

4 Conclusion

A combined experimental and simulation study was conducted on the laser welding process of 6005A aluminum alloy. A composite welding mechanism of “laser preheating + mechanical stirring” was proposed. The key innovations are:

- In welding process design, integrating friction stir welding’s mechanical characteristics. Using a 11 mm diameter stirring head at 1250 r/min, 30° tilt angle, and 0.1 mm pressure control, a “vortex - like” material flow pattern is formed. Laser preheats, mechanical stirring promotes plastic flow, and the 3 mm diameter stirring needle solves oxidation and heat - sensitivity.
- For protective gas ratio, testing an argon - helium - nitrogen (7:2.9:0.1) mixed gas scheme with 15 L/min flow rate improves welding speed and forms a stable protection zone.
- In numerical simulation, establishing a control system with mass, momentum, and energy conservation equations. Using Fortran’s self - developed laser heat source program and metal vapor recoil pressure model. Experimental verification shows welding section morphology from metallographic analysis is consistent with simulation results, providing a new path for high - precision aluminum alloy welding.

Funding

Science and Technology Research Project of Henan Provincial Department of Science and Technology (232102220010); Key Research Project of Higher Education Institutions in Henan Province (23B520017); Zhengzhou Business School New Engineering Innovation Integration Team Project (2021-CXTD-05); The 8th Young Backbone Teacher Training Program Fund Project of Zhengzhou Business University.

Conflicts of interest

The authors declare no conflict of interests.

Data availability statement

All data generated or analysed during this study are included in this published article.

Author contribution statement

Menghua Ma established a multi-reflection laser absorption model for the pinhole and a mathematical model for the molten pool, conducted simulation calculations and experimental verification, analyzed the influence of the laser incident Angle and welding speed on the dynamic behavior of the molten pool, and wrote a paper.

References

1. R. Rout, B.B.V.L. Deepak, B.B. Biswal, et al., Weld seam detection, finding, and setting of process parameters for varying weld gap by the utilization of laser and vision sensor in robotic arc welding, *IEEE Trans. Ind. Electron.* **69** (2022) 622
2. M.F.M. Yusof, M.M. Quazi, S.A.A. Aleem, et al., Identification of weld defect through the application of denoising method to the sound signal acquired during pulse mode laser welding, *Weld. World* **67** (2023) 1267
3. F. Bologna, M. Tannous, D.S.C. Romano, Automatic welding imperfections detection in a smart factory via 2-D laser scanner, *J. Manuf. Process.* **73** (2022) 948
4. J. Peng, H.Q. Xu, X.X. Wang, et al., Numerical simulation of influence of welding speed on dynamic behavior of laser welding molten pool with filler metal, *Chin. J. Lasers* **47** (2020) 137
5. R.S. Huang, J.P. Zou, J.F. Gong, et al., Laser scanning welding pool and plasma dynamic behavior, *Trans. China Weld. Inst.* **41** (2020) 11
6. Z.Y. Yang, Y.C. Fang, J.S. He, Numerical simulation of periodic fluctuation in electron beam welding pool, *J. Mater. Eng.* **47** (2019) 78
7. S.G. Wu, X.Y. Zhou, Z.W. Jiang, et al., Numerical simulation on the temperature field for low-frequency laser oscillation welding of aluminum alloy, *Appl. Laser* **39** (2019) 440
8. N.M. Narayan, S.I. Moqadam, N. Ellendt, et al., Multiphase numerical modeling and investigation of heat transfer for quenching of spherical particles in liquid pool, *Int. J. Therm. Sci.* **186** (2023) 108016
9. S. Park, M. Kim, Y. Koo, et al., Numerical modeling of methane pyrolysis in a bubble column of molten catalysts for clean hydrogen production, *Int. J. Hydrogen Energy* **48** (2023) 7385
10. A.K. Unni, V. Muthukumaran, Modeling of heat transfer, fluid flow, and weld pool dynamics during keyhole laser welding of 316 LN stainless steel using hybrid conical-cylindrical heat source, *Int. J. Adv. Manuf. Technol.* **122** (2022) 3623
11. E.N. Reinheimer, P. Berger, R.G.T. Hagenlocher, Supercritical melt flow in high-speed laser welding and its interdependence with the geometry of the keyhole and the melt pool, *Int. J. Adv. Manuf. Technol.* **131** (2024) 4253
12. Y. Ai, L. Yu, Y. Huang, et al., The investigation of molten pool dynamic behaviors during the “∞” shaped oscillating laser welding of aluminum alloy, *Int. J. Therm. Sci.* **173** (2022) 107350
13. T. Liu, P. Zheng, H. Chen, et al., An attention-based bilinear feature extraction mechanism for fine-grained laser welding molten pool/keyhole defect recognition, *J. Manuf. Process.* **87** (2023) 150

14. W. Muneer, K. Hu, S. He, et al., Microstructure and mechanical properties during dissimilar welding of AA2060-T8 and AA6061-T6 by circular laser beam oscillations, *Mod. Phys. Lett. B* **36** (2022) 2150516
15. C. Yue, A. Yin, D. Huang, Effect of transverse magnetic field on arc characteristics and droplet transfer during laser-MIG hybrid welding of Ti-6Al-4 V, *Int. J. Adv. Manuf. Technol.* **118** (2022) 2481
16. W. Suder, X. Chen, D.R. Sierra, et al., Control of meltpool shape in laser welding, *Weld. World* **68** (2024) 1485
17. Y. Zhao, X. Li, Z. Liu, et al., Stability enhancement of molten pool and keyhole for 2195 Al-Li alloy using fiber-diode laser hybrid welding, *J. Manuf. Process.* **85** (2023) 724
18. X. Xie, W. Huang, J. Zhou, et al., Study on the molten pool behavior and porosity formation mechanism in dual-beam laser welding of aluminum alloy, *J. Laser Appl.* **34** (2022) 22007
19. X. Wang, W. Liu, G. Xu, et al., Numerical analysis of dynamic coupling between the keyhole and molten pool in the rotating laser welding process of aluminum alloy, *Int. J. Adv. Manuf. Technol.* **121** (2022) 5491
20. U.A. Karaniath, M. Vasudevan, Modeling of heat transfer, fluid flow, and weld pool dynamics during keyhole laser welding of 316 LN stainless steel using hybrid conical-cylindrical heat source, *Int. J. Adv. Manuf. Technol.* **122** (2022) 3623
21. G.D.S.R. Gustavo, E.D.S. Magalhaes, et al., S.M.M. de Lima e Silva, Estimating the absorption efficiency in a laser welding process using a nonlinear inverse method, *Int. J. Therm. Sci.* **183** (2023) 107846

Cite this article as: Menghua Ma, A numerical study of dynamic behavior of the molten pool in laser welding of aluminum alloy, *Manufacturing Rev.* **12**, 30 (2025), <https://doi.org/10.1051/mfreview/2025027>